Interfacial Sites in Ag Supported Layered Double Oxide for Dehydrogenation Coupling of Ethanol to *n*-Butanol

Jian Zhang, Kai Shi, Yanru Zhu, Zhe An, Wanning Wang, Xiaodan Ma, Xin Shu,
Hongyan Song, Xu Xiang, and Jing He*[a]

Upgrading of ethanol to *n*-butanol through dehydrogenation coupling has received increasing attention due to the wide application of *n*-butanol. But the enhancement of ethanol dehydrogenation and followed coupling to produce high selectivity to *n*-butanol is still highly desired. Our previous work has reported an acid-base-Ag synergistic catalysis, with Ag particles supported on Mg and Al-containing layered double oxides (Ag/MgAl-LDO). Here, Ag-LDO interfaces have been manipulated for dehydrogenation coupling of ethanol to *n*-

butanol by tailoring the size of Ag particles and the interactions between Ag and LDO. It has been revealed that increasing the population of surface Ag sites at Ag-LDO interfaces promotes not only the dehydrogenation of ethanol to acetaldehyde but also the subsequent aldol condensation of generated acetaldehyde. A selectivity of up to 76% to *n*-butanol with an ethanol conversion of 44% has been achieved on Ag/LDO with abundant interfacial Ag sites, much superior to the state-of-the-art catalysts.

1. Introduction

Production of *n*-butanol has drawn arising attention due to its wide application as a raw bulk chemical in the manufacture of chemical products.[1] Also, *n*-butanol is one of promising alternatives to gasoline as it has 86% energy density compared to gasoline and is easier to store due to its water immiscible nature.[2] Traditionally, *n*-butanol has been produced through fossil-based oxo process (hydroformylation of propylene)[3] or by the fermentation of sugars (acetone-butanol-ethanol process).[1,4] The increased availability of ethanol from biomass[5] drives the interest to upgrade ethanol into more valuable chemicals.[6] Ethanol can undergo C–C formation via Guerbet reaction, offering an economical and sustainable route for *n*-butanol production. So far, it has been generally accepted that the Guerbet reaction involves an aldol-condensation route,[7] even though some researches support the direct condensation mechanism.[8] The aldol-condensation route implies ethanol dehydrogenation to acetaldehyde, aldol condensation of generated acetaldehyde to crotonaldehyde, and hydrogenation of crotonaldehyde to 1-butanol through a hydrogen transfer.

In 1901, Guerbet first reported the dehydrogenation coupling of ethanol to *n*-butanol over barium ethoxide.[7f] Inspired by Guerbet's work, both homogeneous[7d,e,9] and heterogeneous

catalysts[7a,e,10] have been widely developed in upgrading of ethanol to *n*-butanol. Even though excellent performance (> 90% selectivity to *n*-butanol and >20% conversion of ethanol) has been achieved in homogeneous systems in a batch reactor with the addition of extra base (EtONa,[9a,b] nickel or copper hydroxide complexes[9c]), heterogeneous catalyst, including solid acids and/or bases (i.e. oxide or mixed oxides,[10a–e] alkali metal-modified zeolites,[10f] and hydroxyapatite[10g–m]) and supported metals,[10n–s] for continuously upgrading of ethanol to *n*-butanol has been attracting continuous attention due to the potential industrial application. Incorporation of metals in the catalytic system allows the reaction to be carried out at lower temperature with higher ethanol conversion due to the enhanced ethanol dehydrogenation on the metal sites. Cu-CeO$_2$/AC affords a selectivity of 40% towards *n*-butanol with ethanol conversions of 44–46% at 523 K and 2 MPa N$_2$.[10o] Encapsulation of Pd into UiO-66 gives a selectivity of 49.9% toward *n*-butanol with an ethanol conversion of 50.1%.[10p] Ethanol dehydrogenation to acetaldehyde is commonly considered as the rate-determining step in the upgrading of ethanol to *n*-butanol.[10n,o,q–s] In our previous work, the dehydrogenation of ethanol to acetaldehyde has been proposed to be promoted on the metal-support interfacial sites.[11] Despite this progress, the metal-support interfaces in the dehydrogenation coupling of ethanol to *n*-butanol desire more attention. The development of catalyst with tunable interfaces is thus of great importance to enhance the catalytic performance. We previously reported an acid-base-Ag synergistical catalyst with Ag supported on Mg and Al-containing layered double oxides (Ag/MgAl-LDO), derived from Ag loading Mg and Al-containing layered double hydroxides (Ag$^+$/MgAl-LDHs). A selectivity of up to 77% toward *n*-butanol have been achieved with ethanol conversion of 23.2% at 350 °C, 0.1 MPa and selectivity of 60% toward *n*-butanol with ethanol conversion of 45% at 250 °C, 2 MPa.[12]

[a] *J. Zhang, K. Shi, Dr. Y. Zhu, Prof. Z. An, W. Wang, Dr. X. Ma, Dr. X. Shu, Prof. Dr. H. Song, Prof. Dr. X. Xiang, Prof. Dr. J. He*
State Key Laboratory of Chemical Resource Engineering & Beijing Advanced Innovation Center for Soft Matter Science and Engineering
Beijing University of Chemical Technology
Box 98, 15 Beisanhuan Donglu
Beijing 100029 (China)
*E-mail: jinghe@263.net.cn*

Intrigued by our recent discoveries, Ag-LDO interfaces have been manipulated for dehydrogenation coupling of ethanol to *n*-butanol in this work. To the best of our knowledge, this is an original report of interfacial catalysis for upgrading of ethanol to *n*-butanol. A *n*-butanol yield of 39% and a selectivity of 65% toward *n*-butanol have been achieved on Ag-MgAl-LDO with abundant interfacial Ag sites, which is much superior to the state of art catalysts.[10n–s]

2. Results and Discussion

Figure 1 shows the XRD patterns of Mg_4Al-LDHs, Ag^+/Mg_4Al-LDHs, and Ag/Mg_4Al-LDO prepared in this work. For as-prepared or Ag^+ loaded Mg_4Al-LDHs, the reflections characteristic of hydrotalcite-like structure are clearly observed (Figure 1A, a and b). No phase change occurs in the impregnation of as-prepared Mg_4Al-LDHs with $AgNO_3$ aqueous solution. By thermal treatment of Ag^+/Mg_4Al-LDHs under either N_2 (Figure 1B, a) or H_2 (Figure 1B, b–d) atmosphere, both of Mg—Al mixed oxide (MgAl-LDO) (JCPDS: 45-0946) and metallic Ag (JCPDS: 04-0783) are clearly observed for the resulting Ag/Mg_4Al-LDO-N-3h and Ag/Mg_4Al-LDO-H-x. The reflections characteristic of Ag particles become obvious gradually with the thermal treatment time increasing from 1 h to 5 h under H_2 atmosphere (Figure 1B, b–d). In the TEM images (Figure 1C), Ag particles are observed in a maximum distribution at 7.4 nm for Ag/Mg_4Al-LDO-N-3h (Figure 1C, a). But larger Ag particles are observed for $Ag/MgAl$-LDO-H-x, the sample prepared by thermal treatment of Ag^+/Mg_4Al-LDHs under H_2 (Figure 1C, b–d). Increasing thermal treatment time in H_2 obviously results in Ag agglomeration, with the maximum distribution shifting from 17.9 to 34.1 nm. The Ag dispersion was determined by HOT as being 17.2%, 8.3%, 5.6%, and 4.3% (Table 1). Each $Ag/MgAl$-LDO shows a BET surface area around 90 m^2/g (Table 1, entry 1–4).

The surface basicity has been determined by CO_2-TPD technique (Figure 2A). On each Ag loaded Mg_4Al-LDO, a broad CO_2 desorption is observed in the TPD profiles between 50 and 400 °C, which can be deconvoluted into three contributions identified[11,13] as the adsorption of CO_2 on weak basic sites at
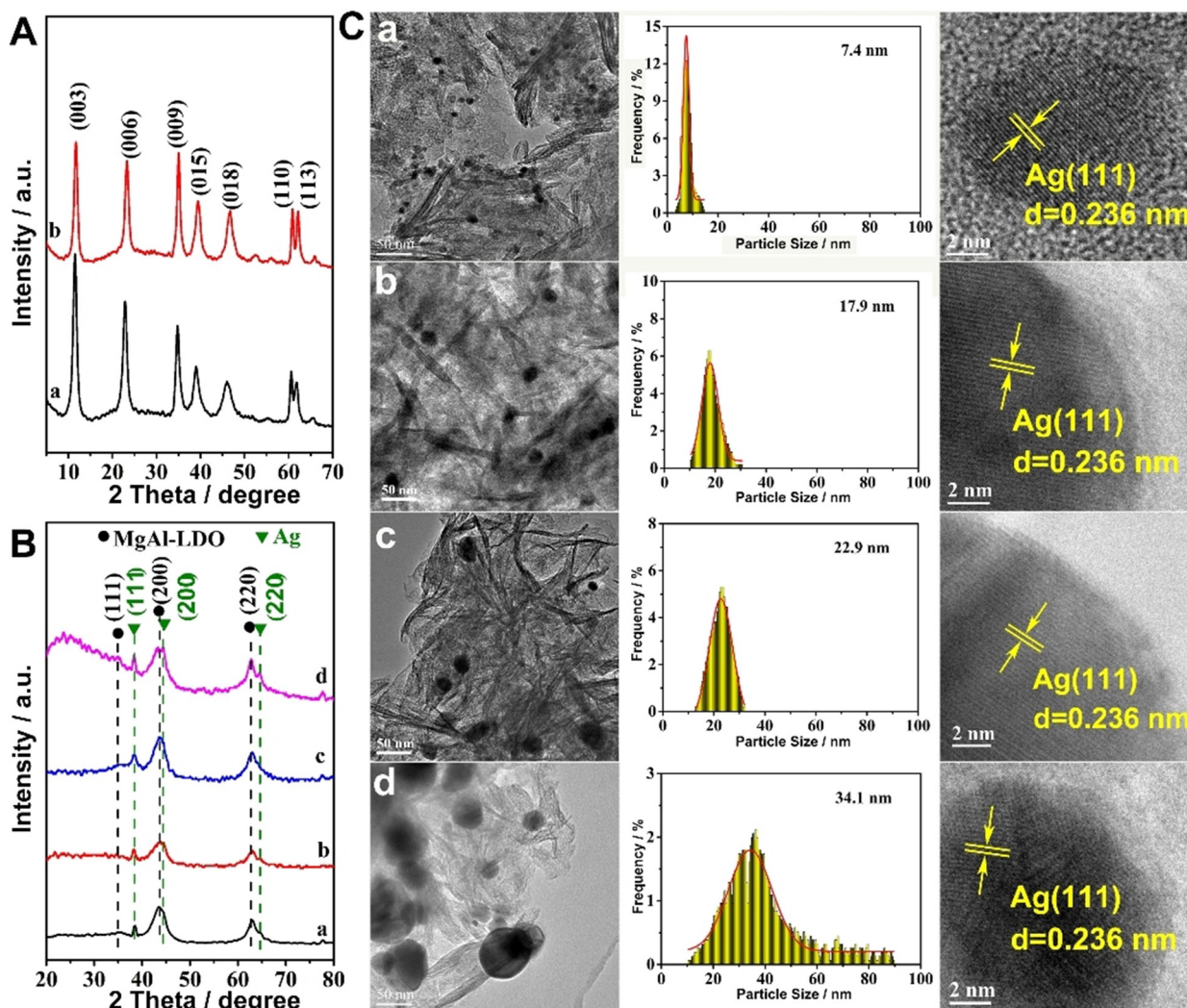

Figure 1. (A) XRD patterns of (a) $Mg_{4.15}Al$-LDHs and (b) Ag^+/Mg_4Al-LDHs; (B) XRD patterns and (C) TEM images, size distribution, and HRTEM images of metallic Ag nanoparticle of (a) Ag/Mg_4Al-LDO-N-3h, (b) Ag/Mg_4Al-LDO-H-1h, (c) Ag/Mg_4Al-LDO-H-3h, and (d) Ag/Mg_4Al-LDO-H-5h.

ChemistryOpen

Full Papers
doi.org/10.1002/open.202000295

Chemistry Europe
European Chemical
Societies Publishing

Table 1. Specific surface area and acid-base properties of Ag supported LDO.

Entry	Samples	S_{BET}/ m²g⁻¹	D_{Ag}/ %	Basic sites[a]/mmol g⁻¹				Basic density/ μmol m²	Acidic sites[b]/ mmol g⁻¹	Acidic density/ μmol m²	Acid/ Base	Ag–O–Al[c]/ %
				weak	medium	strong	total					
1	Ag/Mg₄Al-LDO-N-3h	90.2	17.2	0.16	0.07	0.21	0.44	4.88	0.25	2.77	0.57	29.5
2	Ag/Mg₄Al-LDO-H-1h	88.3	8.3	0.15	0.07	0.22	0.44	4.98	0.26	2.94	0.59	19.7
3	Ag/Mg₄Al-LDO-H-3h	87.7	5.6	0.14	0.07	0.22	0.43	4.90	0.26	2.96	0.60	11.6
4	Ag/Mg₄Al-LDO-H-5h	89.8	4,3	0.17	0.07	0.21	0.45	5.01	0.27	3.01	0.60	8.7
5	Ag/Mg₄Al-LDO*-N-3h	92.4	16.5	0.16	0.08	0.22	0.46	4.98	0.26	2.81	0.57	10.2
6	Ag-Mg₄Al-LDO-H-3h	89.0	61.4	0.15	0.06	0.23	0.44	4.94	0.31	3.48	0.71	39.8

[a] The concentration of weak, medium-strong, and strong basic sites are calculated according to the results of CO_2-TPD and the deconvoluted TPD profile in the temperature region of 50–400 °C. [b] The acidic sites are calculated according to the results of pyridine-FTIR. [c] The Ag–O–Al sites are calculated according to the results of XPS.
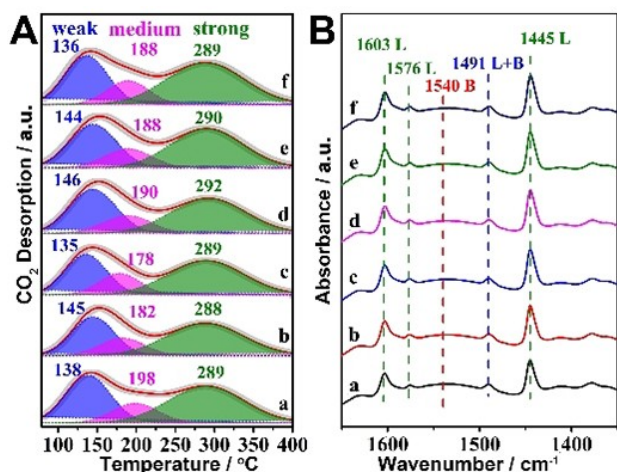
Figure 2. (A) CO_2-TPD profiles and (B) FT-IR spectra of pyridine adsorption for (a) Ag/Mg₄Al-LDO-N-3h, (b) Ag/Mg₄Al-LDO-H-1h, (c) Ag/Mg₄Al-LDO-H-3h, and (d) Ag/Mg₄Al-LDO-H-5h.

< 170 °C, medium-strong basic sites at 170~260 °C, and strong basic sites at > 260 °C. Quantitatively, the total amount and density of base sites are summarized in Table 1. Similar amount and density of basic sites are detected on the Ag/Mg₄Al-LDO prepared by thermal treatment of Ag^+ loaded Mg₄Al-LDHs under either N_2 or H_2 (Table 1, entry 1–4). The surface acidity has been determined by FT-IR spectra of pyridine adsorption (Figure 2B). On the Ag/Mg₄Al-LDO prepared by thermal treatment of Ag^+ loaded Mg₄Al-LDHs under either N_2 or H_2 atmosphere, only Lewis acid sites[14] are observed. The total amount of acid sites shows no marked change with thermal treatment atmosphere or thermal treatment time (Table 1, entry 1–4). All samples show similar ratio of acid to base sites (Table 1, entry 1–4).

Then the Ag/Mg₄Al-LDO, with varied Ag particle size while similar acidic-basic properties, have been applied in the dehydrogenation coupling of ethanol under ambient pressure at 350 °C (Table 2 and Figure 3). An ethanol conversion of 32.6 % is obtained on Ag/Mg₄Al-LDO-N-3h with a selectivity of 61.3 % to n-butanol (Table 2, entry 1). Acetaldehyde and acetate

Table 2. Catalytic results for dehydrogenation coupling of ethanol on LDO supported Ag particles.[a]

Entry	Catalyst	Con./ %	STC[a]	Sel. in liquid product/mol %								$C_{in\ gas\ products}$/ mol %
				Ethyl ether	acetalde-hyde	ethyl acetate	butanal	n-BuOH	i-hexanol	n-hexanol	others	
1	Ag/Mg₄Al-LDO-N3h	32.6 (32.5)	50.8 (50.6)	9.6 (9.2)	14.0 (13.5)	4.1 (4.0)	1.5 (1.4)	61.3 (62.1)	2.1 (2.0)	3.4 (3.5)	4.0 (4.3)	13.8 (14.2)
2	Ag/Mg₄Al-LDO-H-1h	27.9	90.1	10.7	14.2	10.7	2.6	54.5	1.6	2.1	3.6	14.5
3	Ag/Mg₄Al-LDO-H-3h	25.7 (25.5)	123.0 (122.1)	11.2 (10.8)	12.9 (14.3)	12.1 (12.5)	2.1 (2.5)	53.6 (52.5)	1.7 (1.8)	2.9 (2.4)	3.5 (3.2)	15.8 (16.3)
4	Ag/Mg₄Al-LDO-H-5h	17.9	111.6	11.5	15.0	16.8	2.8	47.5	1.4	1.7	3.3	18.8
5	Ag/Mg₄Al-LDO*-N-3h	21.2	34.4	10.9	14.9	16.7	0.7	52.7	0.8	1.0	2.3	14.3
6	Ag-Mg₄Al-LDO-H-3h	43.5 (44.1)	19.0 (19.2)	11.3 (11.8)	1.5 (1.2)	1.3 (1.2)	0.3 (0.4)	75.6 (76.2)	2.0 (1.8)	6.8 (6.2)	1.2 (1.2)	6.4 (5.8)
7	Ag-Mg₄Al-LDO-H-3h[c]	64.3 (63.9)	28.1 (27.9)	11.3 (11.0)	2.5 (2.3)	2.9 (2.8)	0.3 (0.2)	63.4 (63.8)	2.5 (2.8)	13.9 (14.0)	3.2 (3.1)	5.7 (6.2)
8	Ag-Mg₄Al-LDO-H-3h[d]	63.2 (62.8)	27.6 (27.4)	9.2 (9.9)	2.2 (1.8)	1.7 (1.8)	0.5 (0.4)	65.7 (65.6)	3.2 (3.1)	14.8 (14.5)	2.7 (2.9)	6.7 (7.2)

[a] Conversion and selectivity were obtained at initial point; reaction conditions: 500 mg of catalyst, 350 °C, 60 mL min⁻¹ of N_2 (0.1 MPa), LHSV = 6 mL (h g cat)⁻¹. [b] STC for ethanol conversion was calculated by the mole of ethanol converted on per mole of surface Ag per minute. [c] Conversion and selectivity were obtained at initial point; reaction conditions: 250 °C, 2 MPa. [d] Conversion and selectivity were obtained at the steady-state; reaction conditions: 250 °C, 2 MPa. Other products include butyl acetate, ethyl butyrate, 2-ethyl-butanal, hexanal, ethyl 2-ethyl butyrate, butyl butyrate, ethyl caproate, etc. The data in parentheses are the reproduced experimental data.

ChemistryOpen

Full Papers
doi.org/10.1002/open.202000295

Chemistry Europe
European Chemical
Societies Publishing

Figure 3. Stability of (a) Ag/Mg₄Al-LDO-N-3h, (b) Ag/Mg₄Al-LDO-H-1h, (c) Ag/Mg₄Al-LDO-H-3h, and (d) Ag/Mg₄Al-LDO-H-5h. The sphere in dark grey, square in black, star in red, up triangle in blue, and diamond in olive represent for ethanol conversion, selectivity to acetaldehyde, diethy ether, ethyl acetate, and *n*-butanol, respectively.

Figure 4. FT-IR spectra of ethanol adsorption on (A) Ag/Mg₄Al-LDO-N-3h, (B) Ag/Mg₄Al-LDO-H-1h, (C) Ag/Mg₄Al-LDO-H-3h, and (D) Ag/Mg₄Al-LDO-H-5h at 50 °C followed by desorption at 100 °C, 150 °C, 200 °C, 250 °C, 300 °C, 350 °C, and 400 °C.

have also been produced in a selectivity of 14.0% and 4.1% (Table 2, entry 1). But an ethanol conversion of 27.9% with a selectivity of 54.5% to *n*-butanol and a selectivity of 10.7% to acetate is obtained on Ag/Mg₄Al-LDO-H-1h (Table 2, entry 2). Further increasing the Ag particle size disfavors not only the conversion of ethanol but also the formation of *n*-butanol while promotes the selectivity to ethyl acetate (Table 2, entry 3–4). But the site time conversion (STC), determined by ethanol conversion on per surficial Ag atom, first increases with increasing Ag particle size from 7.4 nm to 22.9 nm and then drops slightly with increasing Ag particle size further to 34.1 nm (Table 2, entry 1–4). No obvious changes are observed in the selectivity to ethyl ether with the increase in Ag particle size (Table 2, entry 1–4). 14%–19% of methane and CO_2 are detected in the gaseous products (Table 2, entry 1–4). In our previous work, the acid-base properties showed clearly influence on the selectivity to *n*-butanol.[12] But the great difference in ethanol conversion and selectivity to *n*-butanol is supposed to result from the difference in Ag particle size because the acid-base properties of the catalysts prepared in this work are similar. The catalytic results clearly demonstrates that smaller Ag particles favor the formation of *n*-butanol. The conversion of ethanol and the selectivity to *n*-butanol on each catalyst exhibit no visible change in 12.5 h reaction at 350 °C (Figure 3).

To reveal the role of Ag particle size on dehydrogenation coupling of ethanol, FT-IR spectra of ethanol adsorption/desorption were recorded (Figure 4). In addition to the band assigned[12] to δ_{O-H} of un-dissociated ethanol at 1250 cm⁻¹, 2987–2868 cm⁻¹ to C–H stretching modes, and 1393–1382 cm⁻¹ to δ modes of –CH₃, the bands at 1099–1054 cm⁻¹ assigned to C–O stretching in adsorbed ethoxide and 1617–1604 cm⁻¹ to η¹-adsorbed acetaldehyde have been observed for ethanol adsorption at 50 °C in each case, indicating that the activation of ethanol on Ag/Mg₄Al-LDO occurs through the adsorption of O–H bond, affording ethoxide, followed by dehydrogenation to acetaldehyde. Increasing desorption temperature, the absorption at 50 °C clearly decreases in intensity. The band for C–O

stretching of adsorbed ethoxide at 1099–1077 cm⁻¹ blue shifts to around 1119–1124 cm⁻¹ since 100 °C in each case, and eventually vanishes since 250 °C for Ag/Mg₄Al-LDO-N-3h while 300 °C for Ag/Mg₄Al-LDO-H-1h, Ag/Mg₄Al-LDO-H-3h, and Ag/Mg₄Al-LDO-H-5h. The weak band for η¹-adsorbed acetaldehyde slightly increases in intensity with increasing desorption temperature in each case and becomes dominant since 150 °C for Ag/Mg₄Al-LDO-N-3h and 300 °C for Ag/Mg₄Al-LDO-H-1h, indicating that smaller Ag particles promote the dehydrogenation of ethanol to acetaldehyde, accounting for the higher conversion with decreasing Ag particle size (Table 2, entry 1–4). The bands at 1592–1559 cm⁻¹ and 1416–1443 cm⁻¹ assigned to acetate,[15] which is formed via coupling of ethanol and acetaldehyde[16] or Tishchenko-type disproportionation of two molecules of acetaldehyde,[17] are hardly observed at 50 °C on Ag/Mg₄Al-LDO-N-3h (Figure 4A) and Ag/Mg₄Al-LDO-H-1h (Figure 4B) while clearly observed on Ag/Mg₄Al-LDO-H-3h (Figure 4C) and Ag/Mg₄Al-LDO-H-3h (Figure 4D), demonstrating the strong ability for acetate formation on larger Ag particles. The band assigned to acetate at 1559 cm⁻¹ is hardly observed even at increased desorption temperature for Ag/Mg₄Al-LDO-N-3h (Figure 4A), while emerges since 250 °C for Ag/Mg₄Al-LDO-H-1h (Figure 4B). For Ag/Mg₄Al-LDO-H-3h (Figure 4C) and Ag/Mg₄Al-LDO-H-5h (Figure 4D), the bands for acetate are observed at 1559 and 1381 cm⁻¹ since 50 °C and become dominant since 250 °C. With increasing Ag particle size, the bands to acetate not only are observed at lower temperature, but also become more visible and even dominant in the spectra (Figure 4A–D), indicating that larger Ag particles favors the formation of acetate, accounting for the increase in the selectivity to ethyl acetate. The band at 1456–1451 cm⁻¹ assigned to δ modes of –CH₂[12] is hardly observed on Ag/Mg₄Al-LDO-N-3h (Figure 4A) and Ag/Mg₄Al-LDO-H-1h (Figure 4B), while clearly observed on Ag/Mg₄Al-LDO-H-3h (Figure 4C) and Ag/Mg₄Al-LDO-H-5h (Figure 4D) upon adsorption at 50 °C and following desorption, consistent with the acetate formation on larger Ag particles.

ChemistryOpen

Full Papers
doi.org/10.1002/open.202000295

Chemistry Europe
European Chemical
Societies Publishing

In our previous work, the introduction of Ag particles promoted the aldol condensation of acetaldehyde.[12] The FT-IR spectra of acetaldehyde adsorption at 10 °C on Ag particles in 7.4 nm.

(Ag/Mg4Al-LDO-N-3h) and 34.1 nm (Ag/Mg4Al-LDO-H-5h) were thus recorded (Figure 5). In addition to the bands at 1717 cm^{-1} assigned[12,18] to $\nu(C=O)$, 1463 and 1371 cm^{-1} assigned to $\delta_{as}(CH_3)$ and $\delta_s(CH_3)$, and 1583 cm^{-1} assigned to $\nu_{as}(OCO)$ of acetate, the bands at 1337 cm^{-1} assigned[12,18] to the $\delta_{as}(CH)$ of crotonaldehyde and 1272 cm^{-1} to the $\delta(C\text{-}OH)$ in adsorbed 3-hydroxybutanal are also observed in each case. The intensity of $\delta_s(CH_3)$ at 1371 cm^{-1} is clearly less dominant while the intensity of $\delta(C\text{-}OH)$ in adsorbed 3-hydroxybutanal at 1272 cm^{-1} is more dominant on 7.4 nm Ag (Figure 5, a) than on 34.1 nm Ag (Figure 5, b). That indicates small Ag particles favor the activation of C–H of CH$_3$ in acetaldehyde to promote the aldol condensation, well accounting for the higher selectivity to n-butanol on smaller Ag particles

To make clear the nature of the size effects of Ag particle on the dehydrogenation coupling of ethanol, the electronic state
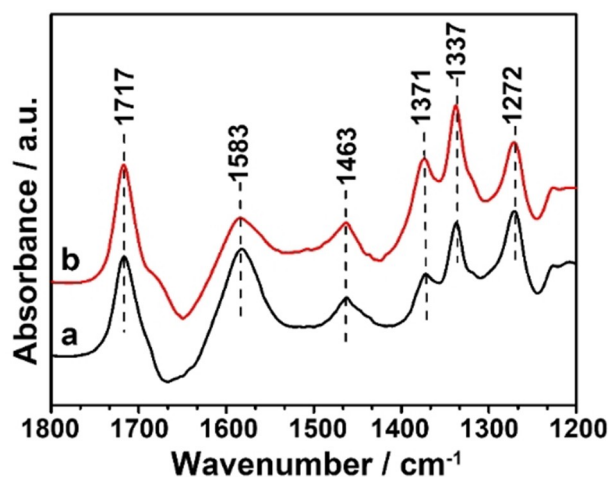
of Ag/Mg4Al-LDO with varied Ag particle size was investigated by XPS technique (Figure 6). In the Ag 3d$_{5/2}$ XPS spectra (Figure 6A), a binding energy at 368.58–368.35 eV assigned[19] to Ag^0 species is clearly observed in each case. Another binding energy is clearly observed at 371.11 eV for Ag/Mg4Al-LDO-N-3h (Figure 6A, a). With an increase in Ag particle size, the binding energy at 371.11 eV shifts to lower value and becomes less obvious (Figure 6A, b–d). So the binding energy higher than Ag^0, observed in this work, probably originate from the Ag sites interacting with Mg4Al-LDO surface. In the Al 2p XPS spectra (Figure 6B), in addition to the binding energy at 74.35–73.95 eV assigned[20] to Mg–O–Al, another binding energy at 75.43–74.91 eV is observed in each case. The peak at 75.43–74.91 eV becomes less obvious with increasing size of Ag particle. In a previous report on Ag doped alumina, an increase in the binding energy of Al 2p has been observed due to the formation of Ag–O–Al chemical bonds.[21] The binding energy at 75.43–74.91 eV is thus proposed to originate from the Al sites interacting with Ag particles. In the Mg 1s XPS spectra (Figure 6C), no obvious change in the binding energy assigned[22] to Mg–O-Mg or Mg–O–Al is observed (Figure 6C) with increasing Ag particle size, further confirming our proposal that the negatively charged Ag sites originates from Ag particles interacting with Al–O sites rather than Mg–O sites. The binding energy of positively charged Ag, such as Ag$_2$O, is lower than that of Ag^0.[19a,c] The binding energy for Ag-O-Mg is also lower than that for Ag^0.[19d] In a previous report on alumina supported Ag,[19b] the binding energy of Ag at interfacial Ag–O–Al sites has been verified to be higher than that for Ag^0, which supports our conclusion. In the O 1s spectra (Figure 6D), three deconvoluted peaks, assigned to absorbed O,[19d] M–O (M=Mg or Al),[19d] and Ag-O,[19c,d] are observed. With the increase of Ag particle size, the deconvoluted area of Ag-O sites declines (Figure 6D), consistent with the decrease in the population of Ag–O–Al sites located at Ag-LDO interface. The fraction of Ag–O–Al interfacial sites, estimated by the deconvoluted area, decreases from 29.5 to 8.7 % with Ag particle size increasing from 7.4 to 34.1 nm (Table 1, entry 1–4).
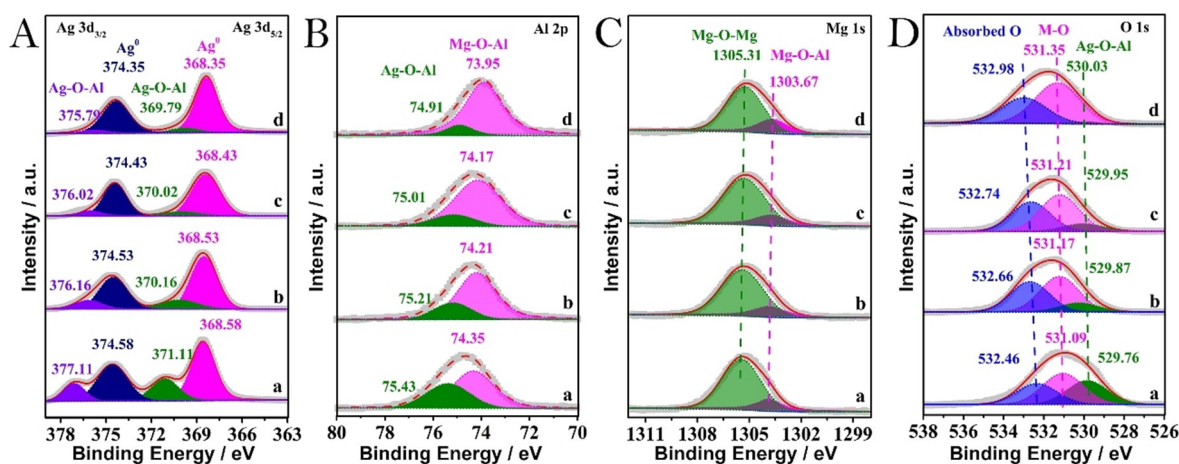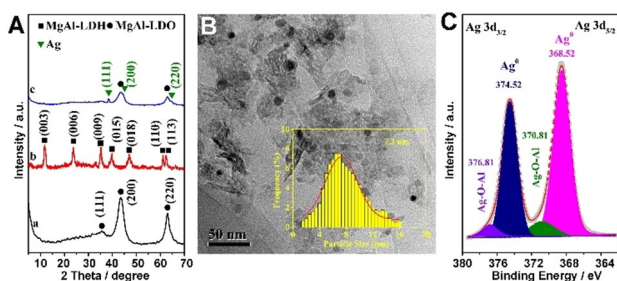

Figure 5. FT-IR spectra of acetaldehyde adsorption at 10 °C on (a) Ag/Mg4Al-LDO7N-3h and (b) Ag/Mg4Al-LDO-H-5h.

Figure 6. XPS spectra of (A) Ag 3d, (B) Al 2p, (C) Mg 1s, and (D) O 1s for (a) Ag/Mg4Al-LDO-N-3h, (b) Ag/Mg4Al-LDO-H-1h, (c) Ag/Mg4Al-LDO-H-3h, and (d) Ag/Mg4Al-LDO-H-5h.

ChemistryOpen

Full Papers
doi.org/10.1002/open.202000295

Chemistry Europe
European Chemical
Societies Publishing

To confirm the key role of interfacial Ag—O—Al sites in the dehydrogenation of ethanol to n-butanol, Ag/Mg$_4$Al-LDO*-N-3h has been prepared for control (Figure 7A). The Mg—O or Al—O in face centered cubic structure of MgO on the LDO surface, unlike the Mg—OH and Al—OH in octahedral structure of Mg(OH)$_2$ on the LDHs surface, provides different chemical environment for Ag$^+$, which might result in the difference in the formation of Ag—O—Al sites during topological transformation from Ag$^+$/LDHs to Ag/LDO. Mg$_4$Al-LDO was first prepared (Figure 7A, a) by thermal treatment of Mg$_4$Al-LDHs under N$_2$ at 400 °C for 3 h and followed by impregnation of Ag$^+$ (Figure 7A, b). The hydrotalcite-like structure was regenerated during the impregnation (Figure 7A, b). Then the regenerated Ag$^+$/Mg$_4$Al-LDHs was re-calcined under N$_2$ at 400 °C for 3 h, producing the Ag/Mg$_4$Al-LDO*-N-3h (Figure 7A, c) with a Ag particle size of 7.3 nm at maximum distribution (Figure 7B). The size distribution of Ag particle size (Figure 7B) and the acid-base properties (Table 1, entry 5) on Ag/Mg$_4$Al-LDO*-N-3h are observed to be similar to those on Ag/Mg$_4$Al-LDO-N-3h. In the XPS spectrum of Ag$_{3d}$ (Figure 7C), interfacial Ag species is observed. The concentration of Ag—O—Al sites is estimated as being 10.2% on Ag/Mg$_4$Al-LDO*-N-3h (Table 1, entry 5), which is much lower than that on Ag/MgAl-LDO-N-3h and similar to that on Ag/MgAl-LDO-H-3h. As a result, in the dehydrogenation coupling to butanol, Ag/Mg$_4$Al-LDO*-N-3h affords an ethanol conversion of 21.2%, with a selectivity of 52.7% to n-butanol (Table 2, entry 5). Acetaldehyde has also been produced in a selectivity of 14.9% and ethyl acetate in 16.7% (Table 2, entry 5). The conversion of ethanol and the selectivity to butanol on Ag/Mg$_4$Al-LDO*-N-3h
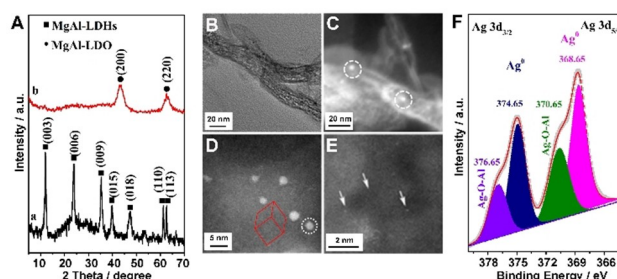
are much lower than that on Ag/Mg$_4$Al-LDO-N-3h, even though Ag/Mg$_4$Al-LDO*-N-3h and Ag/Mg$_4$Al-LDO-N-3h possess similar Ag particle size and acidity-basicity properties. Also, the STC on Ag/Mg$_4$Al-LDO*-N-3h is much lower than that on Ag/Mg$_4$Al-LDO-N-3h, indicating that the interfacial Ag—O—Al sites also promote the ethanol conversion. Ag/Mg$_4$Al-LDO*-N-3h affords similar butanol selectivity to Ag/MgAl-LDO-H-3h due to their similar concentration of Ag—O—Al sites, clearly confirming the crucial role of Ag—O—Al sites in dehydrogenation coupling of ethanol.

Further, Ag-Mg$_4$Al-LDO-H-3h was prepared by thermal treatment of Ag(S$_2$O$_3$)$_2^{3-}$ intercalated Mg$_4$Al-LDHs (Figure 8A, a) under H$_2$ for 3h at 400 °C (Figure 8A, b). HAADF-STEM images show that the cubic Ag particles with maximum distribution at 1.8 nm are located in the interlayer region (Figure 8B-E). Single Ag atoms are also observed in Ag-Mg$_4$Al-LDO-H-3h (Figure 8E). Ag-Mg$_4$Al-LDO-H-3h (Table 1, entry 6) displays similar basic density to all Ag/Mg$_4$Al-LDO, while slightly higher acidic density than Ag/Mg$_4$Al-LDO (Table 1, entry 1–5). From the XPS spectrum of Ag$_{3d}$ (Figure 8F), the fraction of Ag—O—Al sites on Ag-Mg$_4$Al-LDO-H-3h has been estimated as being 39.8% (Table 1, entry 6). Not surprisingly, a selectivity of 75.6% to n-butanol with an ethanol conversion of 43.5% has been achieved on Ag-Mg$_4$Al-LDO-H-3h (Table 2, entry 6), which is higher than all the selectivity reported till now at an ethanol conversion of >40%. But only 19.0 min^{-1} of STC is obtained on Ag-Mg$_4$Al-LDO-H-3h (Table 2, entry 6). For better comparison, the dehydrogenation coupling of ethanol has been carried out at 250 °C and 2 MPa, an ethanol conversion of 55–53% with a selectivity of 63–66% to n-butanol has been achieved (Table 2, entry 7–8), which is superior to the performance of the state of art catalysts. Interestingly, a selectivity of about 15% to n-hexanol has been achieved at 250 °C and 2 MPa (Table 2, entry 7–8).

Then the catalytic performance was plotted as a function of the concentration of Ag—O—Al interfacial sites (Figure 9). Increasing the population of Ag—O—Al interfacial sites promotes the formation of n-butanol while suppresses the formation of acetate. Almost no changes in the selectivity to ethyl ether


Figure 7. (A) XRD patterns of (a) Mg$_4$Al-LDO, (b) Ag$^+$/Mg$_4$Al-LDO, and (c) Ag/Mg$_4$Al-LDO*-N-3h. (B) TEM image and (C) XPS spectrum of Ag 3d for Ag/Mg$_4$Al-LDO*-N-3h. Insertion in (B) is the size distribution of Ag particles.

Figure 8. (A) XRD patterns of (a) Mg$_4$Al-Ag(S$_2$O$_3$)$_2$-LDHs and (b) Ag-Mg$_4$Al-LDO-H-3h. (B–C) STEM image in the view of cross section, (D–E) HAADF-STEM images and (F) XPS spectrum of Ag 3d for Ag-Mg$_4$Al-LDO-H-3h. Insertion in (D) is the shape simulation for Ag particles.

Figure 9. The selectivity to n-butanol, ethyl ether, acetaldehyde, or ethyl acetate and the conversion of ethanol as a function of Ag—O—Al concentration.

ChemistryOpen

Full Papers
doi.org/10.1002/open.202000295

Chemistry Europe
European Chemical
Societies Publishing

have been observed with increasing concentration of Ag−O−Al interfacial sites (Figure 9). Due to the slightly higher acidic sites, higher selectivity to n-butanol (75.6%) and lower selectivity to acetaldehyde (1.5%) than expected have been achieved on Ag-Mg$_4$Al-LDO-H-3h (Figure 9). These results well verify that the interfacial Ag−O−Al sites play a key role in promoting the dehydrogenation coupling of ethanol to n-butanol. But the correlation between STC and Ag−O−Al interfacial sites is still ambiguous, even though the results on Ag/Mg$_4$Al-LDO*-N-and Ag/Mg$_4$Al-LDO-N-3h showed that the Ag−O−Al interfacial sites promoted the ethanol conversion. This result indicates that besides the Ag−O−Al interfacial sites, some other factors on the Ag particle that might affect the ethanol conversion should be taken into consideration.

The catalytic stability in 50 h has been performed with Ag-Mg$_4$Al-LDO-H-3h. Satisfactory stability has been observed in 18 h. A slow decrease in the conversion of ethanol was observed since 18 h and a rapid decrease since 38 h. But the selectivity to n-butanol was well retained in 38 h (Figure 10). Carbon deposition or aggregation of Ag particles might be the reason for the deactivation, which needs further investigation.

3. Conclusions

In summary, the Ag-LDO interfacial sites have been tuned by tailoring the size of Ag particles or changing the preparation method of Ag supported MgAl-LDO. Increasing the interfacial sites clearly enhances the ethanol conversion and aldol condensation while suppresses the formation of ethyl acetate, thus promoting the selectivity to n-butanol. A selectivity of up to 76% to n-butanol with an ethanol conversion of 44% at 350 °C has been achieved on Ag particles with abundant interfacial Ag-LDO sites. More interestingly, a selectivity of 15% to n-hexanol has been achieved at 250 °C under 2 MPa. According to the findings of this work, development of single atom catalyst might be of great importance to enhance the upgrading of ethanol to higher alcohols, such as C$_6$-alcohol. The
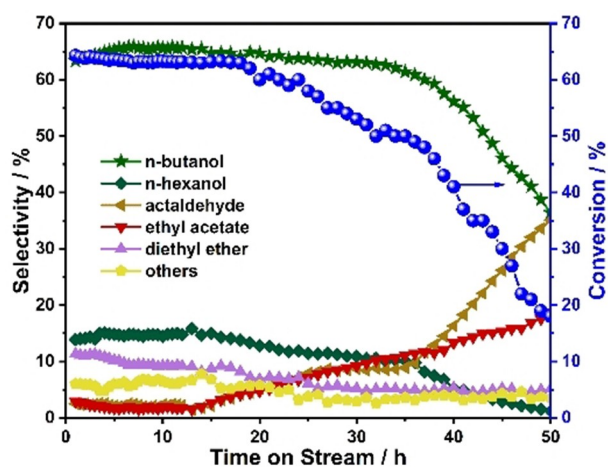
Figure 10. Long-term stability of Ag-Mg$_4$Al-LDO-H-3h in dehydrogenation coupling of ethanol at 250 °C, 2 MPa.

mechanism for deactivation and development of catalyst with long-term stability need further investigation.

Experimental Section

Preparation

Mg$_4$Al-LDHs with Mg/Al molar ratio of 4.15 was prepared as reported in our previous work.[12] Typically, a solution of Mg-(NO$_3$)$_2$·6H$_2$O (0.056 mol) and Al(NO$_3$)$_3$·9H$_2$O (0.014 mol) in 200 mL of deionized water and a solution of NaOH (0.14 mol) and Na$_2$CO$_3$ (0.007 mol) in 200 mL of deionized water were simultaneously added drop-wise to a four-necked flask containing 200 mL of deionized water under constant pH (10.0) at 30 °C. The resulting mixture was aged at 85 °C for 10 h. Then the solid was filtered, washed thoroughly with deionized water till the filtrate is neutral, and dried at 60 °C. Then the Mg$_4$Al-LDHs was thermally treated of at 400 °C for 3h under N$_2$ atmosphere in a rate of 5 °C min^{-1}, producing Mg$_4$Al-LDO.

1 g of Mg$_4$Al-LDHs was impregnated in 1 mL of AgNO$_3$ (4.2 mmol, 6.6 mg) aqueous solution, producing Ag$^+$/Mg$_4$Al-LDHs with Ag loading of 0.42 wt%. Ag/Mg$_4$Al-LDO-N-3h was prepared by thermal treatment of Ag$^+$/Mg$_4$Al-LDHs at 400 °C for 3h under N$_2$ atmosphere. Unless otherwise indicated, the temperature programmed from ambient to reduction temperature in a rate of 5 °C min^{-1}. Ag loading was determined by inductive couple plasma-optical emission spectroscopy (ICP-OES) as being 0.65 wt%. Ag/Mg$_4$Al-LDO-H-x was prepared by thermal treatment of Ag$^+$/Mg$_4$Al-LDHs at 400 °C for varied time under H$_2$ atmosphere, where x represents treatment duration. Ag loading was determined by ICP-OES technique as being in the range of 0.68~0.71 wt%.

Ag$^+$/Mg$_4$Al-LDO with a Ag loading of 0.53 wt% was prepared by impregnation of 1 g Mg$_4$Al-LDO in 1 mL of AgNO$_3$ (5.3 mmol, 8.4 mg) aqueous solution. Ag/Mg$_4$Al-LDO*-N-3h with a Ag loading of 0.75 wt% was prepared by thermal treatment of 0.53 wt% Ag$^+$/Mg$_4$Al-LDO at 400 °C for 3 h under N$_2$ atmosphere.

Mg$_4$Al−Ag(S$_2$O$_3$)$_2$-LDHs was prepared by the reconstruction of Mg$_4$Al-LDO in a Na$_3$Ag(S$_2$O$_3$)$_2$ aqueous solution. Na$_3$Ag(S$_2$O$_3$)$_2$ (0.15 mmol/L Ag) was first prepared by mixing Na$_2$S$_2$O$_3$ and AgNO$_3$ solutions.[23] Typically, 150 mg of Na$_2$S$_2$O$_3$·5H$_2$O was dissolved in 200 mL of deCO$_2$ and deionized water (Solution A) and 10 mg of AgNO$_3$ in 200 mL of deCO$_2$ and deionized water (Solution B). Then Solution B was added drop-by-drop into Solution A with vigorous stirring, forming Na$_3$Ag(S$_2$O$_3$)$_2$ solution. 1 g of Mg$_4$Al-LDO was dispersed in 400 mL of the above Na$_3$Ag(S$_2$O$_3$)$_2$ solution and aged for 24 h at room temperature with slow stirring. All the above procedures were carried out under N$_2$ atmosphere. The solid was filtered, washed with deionized water and anhydrous ethanol for several times, and finally dried at 60 °C in a vacuum oven, affording Mg$_4$Al-Ag(S$_2$O$_3$)$_2$-LDHs. Ag-Mg$_4$Al-LDO·H-3h was prepared by thermal treatment of Mg$_4$Al-Ag(S$_2$O$_3$)$_2$-LDHs at 400 °C for 3h under H$_2$ atmosphere. The Ag loading was determined by ICP-OES method as being 0.73 wt%.

Characterization

Powder X-ray diffraction (XRD) patterns were recorded on Shimadzu XRD-6000 diffractometer operating with Cu Kα radiation (λ= 0.1541) in the range of 3°–80° at a scan rate of 10 ° min^{-1}. The quantitation of Ag, Mg, and Al was carried out by ICP-OES on a Shimadzu ICPS-7500. The low temperature N$_2$ adsorption was performed on a Micromeritics ASAP 2460 and specific surface area

ChemistryOpen

Full Papers
doi.org/10.1002/open.202000295

Chemistry Europe
European Chemical
Societies Publishing

was calculated using Brunauer-Emmett-Teller (BET) method. TEM and HRTEM images were taken on a Tecnai G^2 F30 operating at 300 kV. The high-angle annular dark field (HAADF)-scanning transmission electron microscopic (STEM) images were taken on a JEM-ARM 200F electron microscope capable of subangstrom resolution. The Ag dispersion was determined by hydrogen-oxygen titration (HOT) on a Micrometric ChemiSorb 2920 chemisorption system with a thermal conductivity detector (TCD). 100 mg of Ag loaded sample was pre-treated at 350 °C for 1 h under 20 mL min^{-1} of He and then cooled to 180 °C in the flow of He. Afterwards, O$_2$ pulses were introduced into the system until saturation and then the absorbed oxygen was titrated by introducing pulses of H$_2$ at 180 °C. The Ag dispersion was calculated as follows:

$$D_{Ag} = 2 \times \text{amount of consumed } H_2/N_{total} \text{ (by ICP)} \times 100\% \quad (1)$$

The X-ray photoelectron spectra (XPS) were recorded on an AXIS SUPRA X-ray photoelectron spectrometer equipped with monochromated Al-K X-ray source (1486.6 eV) at a pass energy of 40 eV. C 1s peak at 284.6 eV was used as a calibration peak. Since the Auger peak of Mg overlaps with the peak of Ag 3d$_{3/2}$, the peak for Ag 3d was obtained by subtracting the Auger peak of Mg from the original data in this work. The population of Ag–O–Al sites was calculated as follows:

$$\text{Ag–O–Al } \% = A_{Ag–O–Al}/(A_{Ag–O–Al} + A_{Ag}^0) \times 100\% \quad (2)$$

where A_i was the deconvoluted area for Ag–O–Al or Ag^0.

CO$_2$-temperature programmed desorption (TPD) experiment was performed on a Micrometric ChemiSorb 2920. Typically, 100 mg of sample was loaded in a U-type quartz tube reactor and pre-treated at 400 °C for 1 h under He mixture (40 mL min^{-1}). Afterward, the sample was cooled to 50 °C in the flow of He (40 mL min^{-1}) and then CO$_2$ (20 mL min^{-1}) was fed into the reactor until saturation. A flow of He (40 mL min^{-1}) was subsequently fed for 0.5 h to desorb weakly physical adsorption. CO$_2$-TPD was carried out under He (40 mL min^{-1}) from 50 to 400 °C with a temperature-programmed rate of 10 °C min^{-1}.

The Fourier-transform infrared spectra (FT-IR) of pyridine, acetaldehyde, or ethanol adsorption with self-support sample wafer were recorded on an iS50 FT-IR (NICOLET) spectrometer equipped a mercury-cadmium-telluride (MCT) detector, with a resolution of 4 cm^{-1} and 64 scans. The to-be-measured sample was firstly loaded into in-situ IR cell, then pre-treated under Ar (40 mL min^{-1}) at 400 °C for 1 h, and cooled in Ar. For pyridine adsorption, the system was first evacuated and the spectrum for background was recorded at 50 °C. The sample was then exposed to pyridine vapor until adsorption saturation, and then the adsorbed pyridine was desorbed at 150 °C until the spectra showed no change. The spectrum was recorded. The Lewis and Brønsted acid sites was quantitatively caculated as following equation:[14]

$$C_L = 1.41 \times r^2/w \times A_{1440} \quad (3)$$

$$C_B = 1.88 \times r^2/w \times A_{1540} \quad (4)$$

where C_L and C_B are concentrations of Lewis acid sites and Brønsted acid sites (μmol g^{-1}), A_{1440} and A_{1540} are integrated areas of the bands at 1440 and 1540 cm^{-1}, r is the wafer radius (cm), and w is the wafer weight (g). For acetaldehyde adsorption, the system was first evacuated and the spectrum for background was recorded at 10 °C. The sample was then exposed to acetaldehyde vapor until adsorption saturation, and then purged with Ar until the spectra

showed no change. The spectrum was recorded. For ethanol adsorption-desorption, the spectrum for background was recorded at 400 °C, 350 °C, 300 °C, 250 °C, 200 °C, 150 °C, 100 °C, and 50 °C in the cooling from 400 to 50 °C after the pre-treatment. Subsequently, the ethanol was bubbled into the system by Ar (20 mL min^{-1}) at 50 °C for 40 min, and then purged with Ar (20 mL min^{-1}) until the spectra showed no change. The spectrum for ethanol adsorption at 50 °C was recorded. Then the temperature was increased to 100 °C under Ar with a heating rate of 10 °C min^{-1} and maintained at 100 °C for 10 min. The spectrum for ethanol desorption at 100 °C was recorded. The spectrum for ethanol desorption at 150 °C, 200 °C, 250 °C, 300 °C, 350 °C, or 400 °C was recorded in the same procedure.

Catalytic Tests

The dehydrogenation coupling of ethanol was carried out in a fixed-bed reactor as the procedures described in our previous work with a stainless steel tubular reactor in an external diameter of 10 mm and a length of 38 cm.[12] Typically, 0.5 g of catalyst (20–40 mesh) was loaded into the constant temperature zone of the reactor. Prior to the reaction, the catalyst was pretreated in situ with N$_2$ (40 mL min^{-1}) at 400 °C for 1 h and then cooled to 350 °C. The N$_2$ gas flow was set to 60 mL min^{-1}. The chromatographically pure ethanol was pumped into a vaporizing chamber (150 °C) at a flow rate of 50 μL min^{-1}, where ethanol vapor and N$_2$ were mixed, and then into the reaction system. The pipeline behind the reactor was heated to keep at 200 °C. The products were analyzed quantitatively by GC (Shimadzu, 2014C) with a flame ionization detector (FID) and a GSBP-INOWAX column (30 m, 0.25 mm inner diameter). The ethanol conversion and product selectivity were calculated as follows:

$$\text{Con.}\% = (F_{in} - F_{unreacted})/F_{in} \times 100\% \quad (5)$$

$$\text{Sel.}\% = C_{in \text{ specific product}}/C_{in \text{ all liquid products}} \times 100\% \quad (6)$$

wherein, F_{in} and $F_{unreacted}$ are the moles of initial ethanol and unreacted ethanol; $C_{in \text{ ethanol reacted}}$ were calculated based on the moles of carbon in all liquid and gaseous products; $C_{in \text{ specific product}}$ and $C_{in \text{ all liquid products}}$ were the moles of carbon in the specific product and all liquid products. Each catalyst exhibited good stability in a 12.5 h test, showing traceable carbon deposition rate. Therefore, the carbon balance is close to 100% and the $C_{in \text{ gas products}}$ % is calculated as follows:

$$C_{in \text{ gas products}} \% = (1 - C_{in \text{ all liquid products}}/C_{in \text{ ethanol reacted}}) \times 100\% \quad (7).$$

Mass transfer limitations on Ag/Mg$_4$Al-LDO-N-3h at 623 K, 0.1 MPa with ethanol conversion of 32% were calculated using the Mears and Weisz-Prater analyses.[24] Mears Criterion for external diffusion and Weisz-Prater Criterion for internal diffusion were $1.1 \times 10^{-7} < 0.15$ and $0.1 < 1$, respectively, suggesting the absence of diffusion limitation in this work.

Acknowledgements

Conflict of Interest

The authors declare no conflict of interest.

[1] B. Ndaba, I. Chiyanzu, S. Marx, *Biotechnol. Rep.* **2015**, *8*, 1–9.

[2] a) W. R. d. S. Trindade, R. G. d. Santos, *Renewable Sustainable Energy Rev.* **2017**, *69*, 642–651; b) C. Jin, M. Yao, H. Liu, C.-f. F. Lee, J. Ji, *Renewable Sustainable Energy Rev.* **2011**, *15*, 4080–4106.

[3] U. C. Corp, GB, GB815566A, **1957**.

[4] a) W. Charles, GB, GB191504845A, **1915**; b) N. P. Nguyen, C. Raynaud, I. Meynial-Salles, P. Soucaille, *Nat. Commun.* **2018**, *9*, 3682.

[5] G. W. Huber, S. Iborra, A. Corma, *Chem. Rev.* **2006**, *106*, 4044–4098.

[6] J. Sun, Y. Wang, *ACS Catal.* **2014**, *4*, 1078–1090.

[7] a) J. T. Kozlowski, R. J. Davis, *ACS Catal.* **2013**, *3*, 1588–1600; b) D. Gabriëls, W. Y. Hernández, B. Sels, P. V. D. Voort, A. Verberckmoes, *Catal. Sci. Technol.* **2015**, *5*, 3876–3902; c) A. Galadima, O. Muraza, *Ind. Eng. Chem. Res.* **2015**, *54*, 7181–7194; d) H. Aitchison, R. L. Wingad, D. F. Wass, *ACS Catal.* **2016**, *6*, 7125–7132; e) X. Wu, G. Fang, Y. Tong, D. Jiang, Z. Liang, W. Leng, L. Liu, P. Tu, H. Wang, J. Ni, X. Li, *ChemSusChem* **2018**, *11*, 71–85; f) M. Guerbet, *J. Chem. Soc. Abstr.* **1901**, *80*, l625.

[8] a) A. Ndou, *Appl. Catal. A* **2003**, *251*, 337–345; b) T. Tsuchida, S. Sakuma, T. Takeguchi, W. Ueda, *Ind. Eng. Chem. Res.* **2006**, *45*, 8634–8642; c) J. Scalbert, F. Thibault-Starzyk, R. Jacquot, D. Morvan, F. Meunier, *J. Catal.* **2014**, *311*, 28–32.

[9] a) G. R. Dowson, M. F. Haddow, J. Lee, R. L. Wingad, D. F. Wass, *Angew. Chem. Int. Ed.* **2013**, *52*, 9005–9008; *Angew. Chem.* **2013**, *125*, 9175–9178; b) S. Fu, Z. Shao, Y. Wang, Q. Liu, *J. Am. Chem. Soc.* **2017**, *139*, 11941–11948; c) S. Chakraborty, P. E. Piszel, C. E. Hayes, R. T. Baker, W. D. Jones, *J. Am. Chem. Soc.* **2015**, *137*, 14264–14267.

[10] a) J. I. D. Cosimo, C. R. Apesteguía, M. J. L. Ginés, E. Iglesia, *J. Catal.* **2000**, *190*, 261–275; b) M. León, E. Díaz, S. Ordóñez, *Catal. Today* **2011**, *164*, 436–442; c) D. L. Carvalho, R. R. de Avillez, M. T. Rodrigues, L. E. P. Borges, L. G. Appel, *Appl. Catal. A* **2012**, *415–416*, 96–100; d) T. W. Birky, J. T. Kozlowski, R. J. Davis, *J. Catal.* **2013**, *298*, 130–137; e) S. Hanspal, Z. D. Young, H. Shou, R. J. Davis, *ACS Catal.* **2015**, *5*, 1737–1746; f) C. Yang, Z. Meng, *J. Catal.* **1993**, *142*, 37–44; g) T. Tsuchida, J. Kubo, T. Yoshioka, S. Sakuma, T. Takeguchi, W. Ueda, *J. Catal.* **2008**, *259*, 183–189; h) S. Ogo, A. Onda, K. Yanagisawa, *Appl. Catal. A* **2011**, *402*, 188–195; i) T. Tsuchida, S. Sakuma, T. Takeguchi, W. Ueda, *Ind. Eng. Chem. Res.* **2006**, *45*, 8634–8642; j) C. R. Ho, S. Shylesh, A. T. Bell, *ACS Catal.* **2016**, *6*, 939–948; k) T. Moteki, D. W. Flaherty, *ACS Catal.* **2016**, *6*, 4170–4183; l) S. Ogo, A. Onda, Y. Iwasa, K. Hara, A. Fukuoka, K. Yanagisawa, *J. Catal.* **2012**, *296*, 24–30; m) M. B. Osman, J. M. Krafft, C. Thomas, T. Yoshioka, J. Kubo, G. Costentin, *ChemCatChem* **2019**, *11*, 1765–1778; n) J. Pang, M. Zheng, L. He, L. Li, X. Pan, A. Wang, X. Wang, T. Zhang, *J. Catal.* **2016**, *344*, 184–193; o) D. Jiang, X. Wu, J. Mao, J. Ni, X. Li, *Chem. Commun.* **2016**, *52*, 13749–13752; p) D. Jiang, G. Fang, Y. Tong, X. Wu, Y. Wang, D. Hong, W. Leng, Z. Liang, P. Tu, L. Liu, K. Xu, J. Ni, X. Li, *ACS Catal.* **2018**, *8*, 11973–11978; q) X. Wu, G. Fang, Z. Liang, W. Leng, K. Xu, D. Jiang, J. Ni, X. Li, *Catal. Commun.* **2017**, *100*, 15–18; r) P. A. Kots, A. V. Zabilska, Y. V. Grigor'ev, I. I. Ivanova, *Petrol. Chem.* **2019**, *59*, 925–934; s) C. Lopez-Olmos, A. Guerrero-Ruiz, I. Rodríguez-Ramos, *Catal. Today* **2019**, https://doi.org/10.1016/j.cattod.2019.1005.1058.

[11] a) J. Zhang, Z. An, Y. Zhu, X. Shu, H. Song, Y. Jiang, W. Wang, X. Xiang, L. Xu, J. He, *ACS Catal.* **2019**, *9*, 11438–11446; b) J. Zhang, W. Yan, Z. An, H. Song, J. He, *ACS Sustainable Chem. Eng.* **2018**, *6*, 7313–7324.

[12] J. Zhang, K. Shi, Z. An, Y. Zhu, X. Shu, H. Song, X. Xiang, J. He, *Ind. Eng. Chem. Res.* **2020**, *59*, 3342–3350.

[13] O. D. Pavel, D. Tichit, I. C. Marcu, *Appl. Clay Sci.* **2012**, *61*, 52–58.

[14] C. A. Emeis, *J. Catal.* **1993**, *141*, 347–354.

[15] J. V. Ochoa, C. Trevisanut, J. M. M. Millet, G. Busca, F. Cavani, *J. Phys. Chem. C* **2013**, *117*, 23908–23918.

[16] M. Nielsen, H. Junge, A. Kammer, M. Beller, *Angew. Chem. Int. Ed.* **2012**, *51*, 5711–5713.

[17] H. Horino, T. Ito, A. Yamamoto, *Chem. Lett.* **1978**, *1*, 17–20.

[18] A. K. P. Mann, Z. Wu, F. C. Calaza, S. H. Overbury, *ACS Catal.* **2014**, *4*, 2437–2448.

[19] a) E. Sekera, J. Cavataioa, E. Gularia, P. Lorpongpaiboonb, S. Osuwan, *Appl. Catal. A* **1999**, *183*, 121–134; b) X. She, M. Flytzani-Stephanopoulos, *J. Catal.* **2006**, *237*, 79–93; c) V. K. Kaushik, *J. Electron. Spectros. Relat. Phenomena* **1991**, *56*, 273–277; d) Y. Cai, D. Wu, X. Zhu, W. Wang, F. Tan, J. Chen, X. Qiao, X. Qiu, *Ceram. Int.* **2017**, *43*, 1066–1072.

[20] Y. Kameshima, A. Yasumori, K. Okada, *Surf. Sci. Soc. Jpn.* **2000**, *21*, 481–487.

[21] D. Zou, X. Chen, E. Drioli, X. Ke, M. Qiu, Y. Fan, *J. Membr. Sci.* **2020**, *593*.

[22] a) S. Ardizzone, C. L. Bianchi, M. Fadoni, B. Vercelli, *Appl. Surf. Sci.* **1997**, *119*, 253–259; b) J. S. Corneille, J.-W. He, D. W. Goodman, *Surf. Sci.* **1994**, *306*, 269–278.

[23] M. S. Bhadraver, *Bull. Chem. Soc. Jpn.* **1962**, *35*, 1939–1941.

[24] a) D. E. Mears, *Ind. Eng. Chem. Process Des. Dev.* **1971**, *10*, 541–547; b) P. B. Weisz, C. D. Prater, *Adv. Catal.* **1954**, *6*, 143–196.